

# 3D Seismic-Reflection Analysis Using Image J, Manual Interpretation and Automated Fault Extraction of Polygonal Fault Systems in Great South Basin, New Zealand

Ulandari M Ali<sup>1</sup>, Stefan Back<sup>2</sup>

<sup>1,2</sup> (Department of Geology – Energy and Mineral Resources Group, Rheinisch-Westfälische Technische Hochschule (RWTH) Aachen University, Germany)

---

## **Abstract:**

The main purpose of this paper is to compare three techniques to map directionality of polygonal fault systems (PFS) in Great South Basin (GSB), New Zealand. While the interpretation of polygonal to circular faults is often challenging, their identification is crucial in order to obtain detail subsurface condition. This study used 3D seismic-reflection analysis as a key tool to obtain fault geometry and directionality. The methods applied for polygonal faults mapping are Image J, manual interpretation and automated fault extraction. The time slices delineate the changes of PFS morphology through time. With the variance time slices, a preferred direction of the fault's structures can be computed by Image J directionality. The conventional method of fault interpretation such as manual interpretation allows us to do manual picking and construct the fault's plane. However, for the data containing a high number of faults, this method becomes less efficient. Hence, there are only several major faults which were chosen based on their dominant and/ visible directions. On the other hand, automated fault extraction using ant tracking attribute is able to enhance the clarity of polygonal faults and provide more fault data that are hard to observe in the 3D data set. Therefore, the orientation obtained from this method are more varied. The variation of PFS directionality from three approaches might indicates the limitation of each method. In addition, the development of polygonal fault planform was also presented in time interval which related to the stress perturbation and the presence of pockmarks.

**Keywords:** polygonal faults, orientation, planform geometry, variance, attribute, pockmarks

---

Date of Submission: 04-06-2023

Date of Acceptance: 17-06-2023

---

## **I. Introduction**

Polygonal Fault System (PFS) can be described as layer bound faults forming a network limited to a specific stratigraphic unit<sup>1</sup>. PFS commonly occur in slope settings along continental margins and some are also developed in abyssal basins, foreland basins and intracratonic basins<sup>2</sup>. PFS were first recognized as non-tectonic features in the 1980s by using 2D seismic data<sup>3,4,5</sup>. In the 1990s, PFS were identified on 3D seismic survey data in many settings, with the first in Paleogene mudstones of the North Sea Basin<sup>6,7</sup>.

The Great South Basin is located offshore at the south-eastern margin of New Zealand (Figure 1). This basin has undergone multiple tectonic phases. The breakup of Gondwana in the Early Cretaceous resulted in the extension, crustal thinning, rifting and sedimentary fill of the basin<sup>8</sup>. The extensive polygonal faults are situated on the post-rift passive margin (in Eocene to Oligocene stratigraphic interval) with a length of few hundreds to thousands of meters and are not affected by any tectonic processes. The identification of the age and lithology within the layer of the fault system is based on data from nearby well e.g., Pakaha-1<sup>9</sup>. The presence of the polygonal to circular faults can be caused by several mechanisms including: fluid escape features (e.g., pockmarks), gravity collapse, density inversion, compactional loading, sediment dewatering and volume loss associated with compaction, dissolution of hydrous mineral phases during burial and biological growth forming mound structures<sup>1,10,11,12,13,14,15</sup>.

The subsurface interpretation is challenging especially data containing a high number of faults. However, by the development of 3D seismic data, the result obtained will be useful to illustrate the subsurface condition. In this study, 3D seismic-reflection analysis is used as a key tool to obtain the fault geometry and directionality. The manual interpretation and automated fault extraction were generated in 3D area in five different places of GSB. Additionally, Image J software was also applied to analyse a general fault directionality in those five individual target areas, with the objective of comparing and analysing the results from three different techniques.

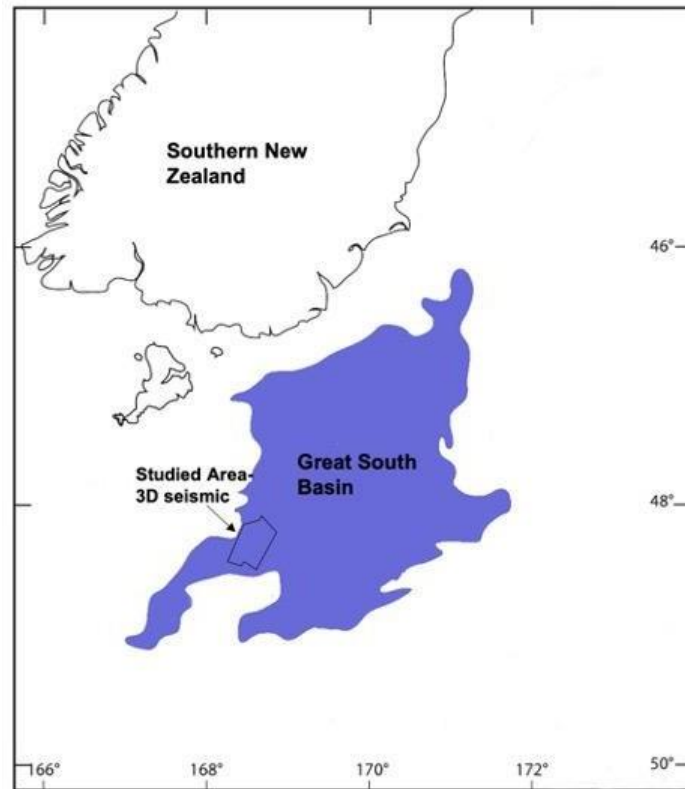


**Fig. 1** Location of GSB and studied area.

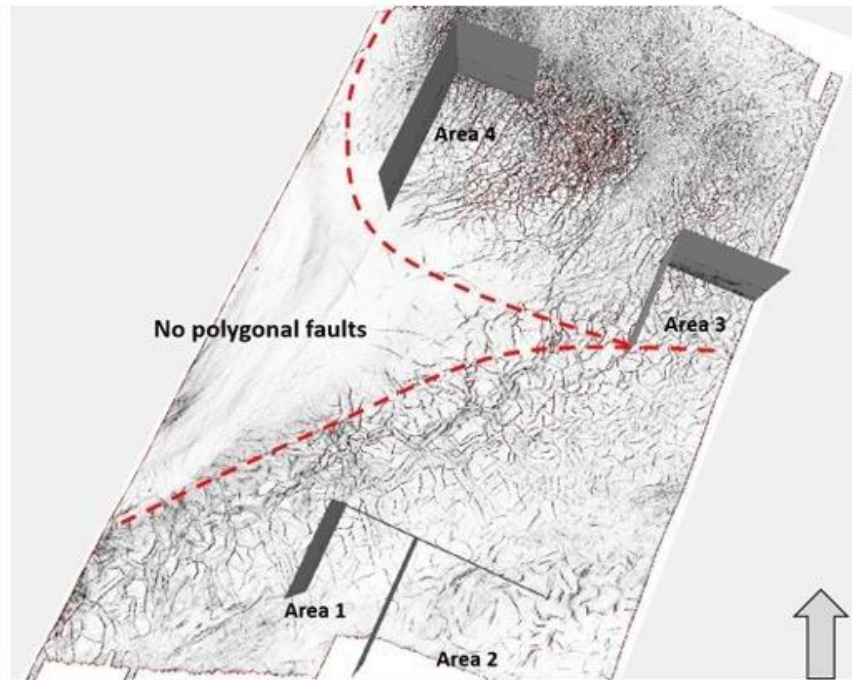
## II. Material And Methods

In this study, there are five virtual cropped sub-volumes chosen for detailed analysis based on their fault's morphology, slope, and also general orientation (Figure 2). The stratigraphic units of the areas can be divided into three: unit 1 consists of an upper and a lower part (below the clastic progradational unit, Figure 3a). The lower part of unit 1 consists of deltaic progradation clinoforms and the overlying Waipawa Shale Formation, whereas the upper part is dominated by shelfal sandy siltstone with silty shales from the Laing Formation<sup>9</sup>. Unit 2 covers the Tucker Formation to the Marshall unconformity as the upper boundary (Figure 3b). The Tucker Formation is dominated by marl sedimentation<sup>9</sup>. Unit 3 is marked by hummocky reflections (Figure 3c) interpreted as the sediment drift sheets<sup>16</sup>, and the transition from marl-sedimentation to chert and carbonates-rich oozes of the Penrod Formation<sup>9</sup>.

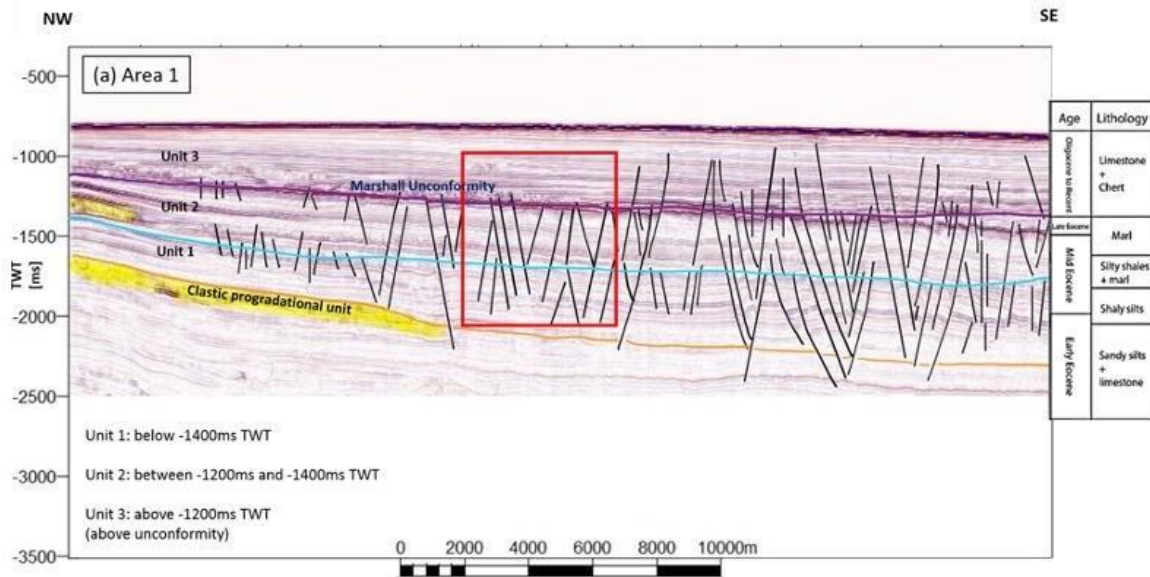
The progradation unit trends from the NW to SE. The northern PFS are located in the shallower stratigraphic units while the southern PFS extend to the deeper layers. The PFS are observed in different slope settings in which the PFS of area 3 are found in the steepest slope, whereas the PFS in area 1, 2 and 4 are located in gentler slope areas.

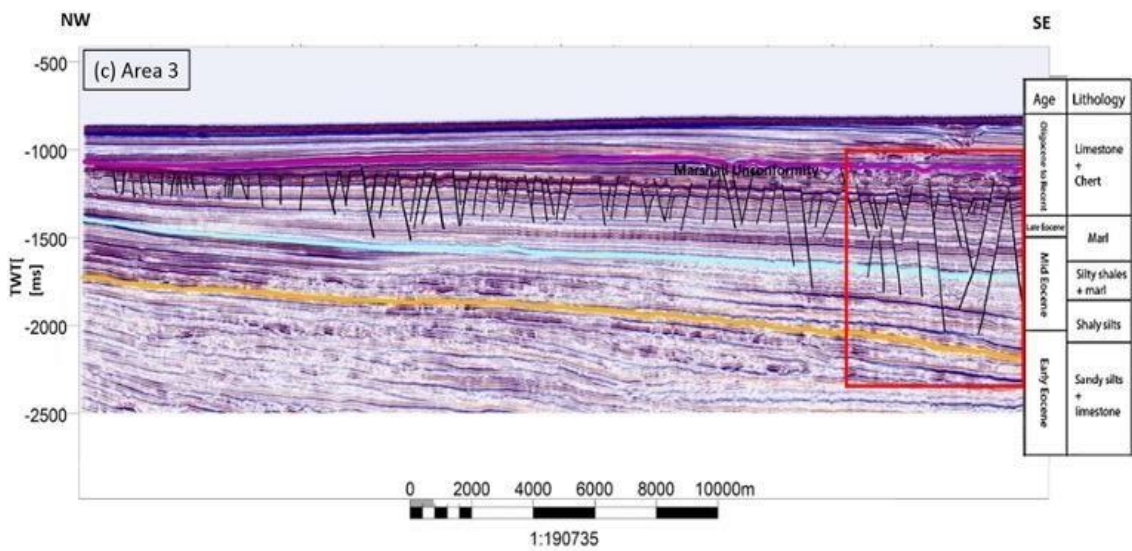
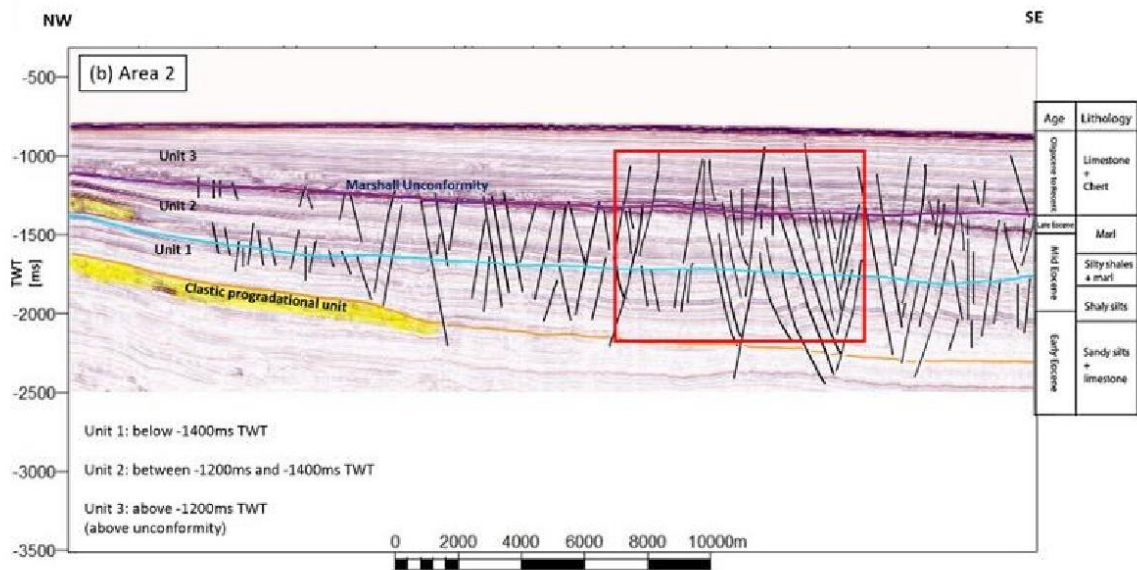
Faults forming PFS are typically normal faults with individual faults that tend to be either planar faults or gentle listric faults caused by the increasing of vertical stress that resulted a compactional flattening of the fault planes<sup>17</sup>. The polygonal faults in the chosen areas have a consistent dip in the range of  $48^{\circ}$  -  $52^{\circ}$  due to a fairly homogenous composition and rate of compaction of the fine-grained deposits, whereas the strikes vary significantly.

The PFS in area 1 and 2 are well-developed. These areas have a thicker sediment cover from about -1000ms to -2300ms TWT. Towards the north, the size of the PFS is decreasing. In area 3, the PFS is developed over an interval 800ms thick, whereas in area 4, the PFS cover an interval of 150 – 300ms thick is situated in the shallower tier prior to the Marshall Unconformity.



**Fig. 2** 3D seismic survey map with the red dash line represents of the area where the polygonal faults developed. There are four study areas which will be analysed further. Note: area 4 is sub-divided into two (4.1 and 4.2) due to its planform pattern and maturity.





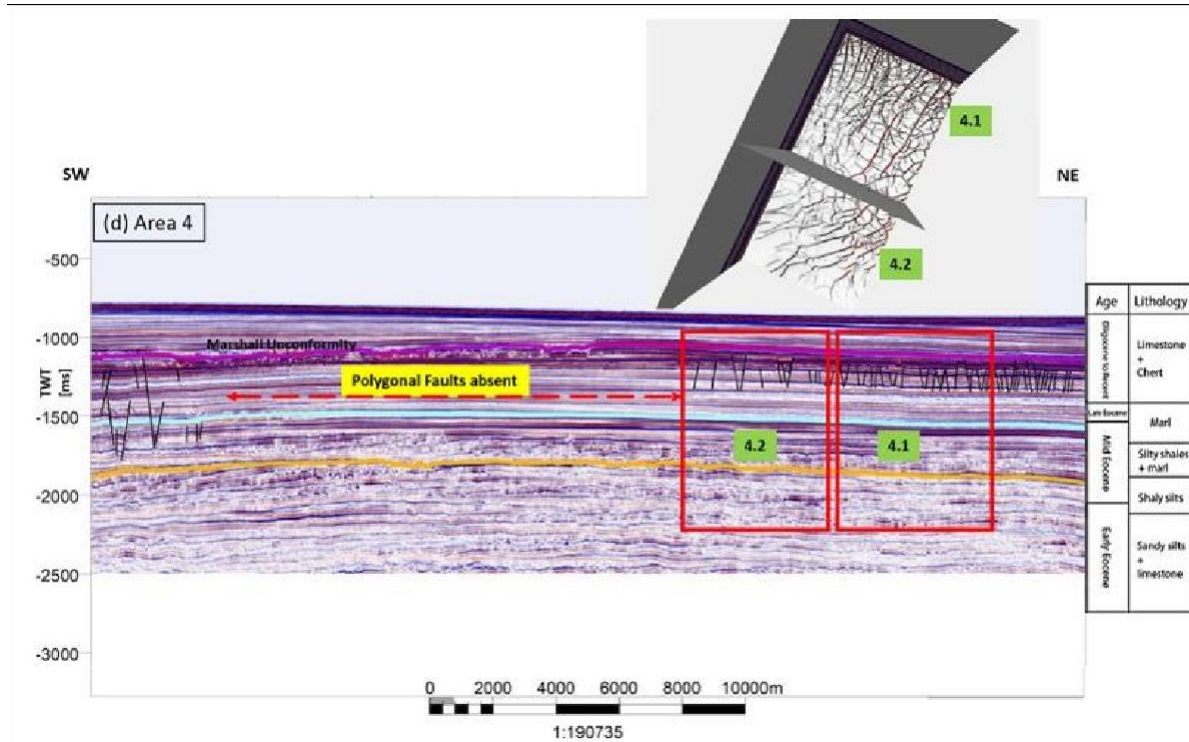


**Fig. 3** (a-d): seismic sections of study areas. The red rectangles indicate the PFS of the area of interest. The age and lithology were taken from Pakaha-1 well, modified from Morley *et al.*, 2017. For the map location refer to Figure 2.

The variance attributes of each sub-volumes were then created and grouped into several intervals based on time slices (Figure 4). Variance attribute images of each time slice in the range of -1000ms to -2300ms TWT were processed with Image J to obtain a preferred direction of faults. Image J calculates a histogram which indicates the number of structures in the given direction of the image. The image with fully isotropic content is expected to generate a flat histogram, while an image with a preferential orientation is expected to give a histogram with a peak at that point<sup>18</sup>. The results from Image J can also be used as a guidance to see the general orientation of PFS before manual picking.

An important part of the fault analysis process was seismic interpretation by Schlumberger Petrel Software which provides the structural framework information for further analysis. The conventional way of doing seismic data interpretation is manual picking on the 3D seismic data. However, it is quite complex due to the quality of data and a high number of polygonal faults in the study areas. Therefore, only 10 to 20 faults were chosen per sub-volume based on the visible directions or dominant orientation that were identified. Manual picking was also helpful to visualise the trend of polygonal faults in each time slice. Seismic attributes applied including variance and ant tracker (Figure 5). These attributes are helpful to enhance the clarity of the seismic reflectors or its geometrical characteristics<sup>19</sup>. The ant tracking always produced a better trend visualisation of faults which are not immediately visible on a seismic slice. From ant tracking data, the polygonal fault can be extracted automatically and the orientations (dip azimuth and dip) can be calculated. The development of the polygonal faults is not directly affected by sediment deposition; hence the geometric description and orientation of polygonal faults are illustrated from the younger layer (above the Marshall Unconformity) to the older layer which lies below the unconformity. The reason is to see how the PFS are recorded and have developed within the stratigraphy.

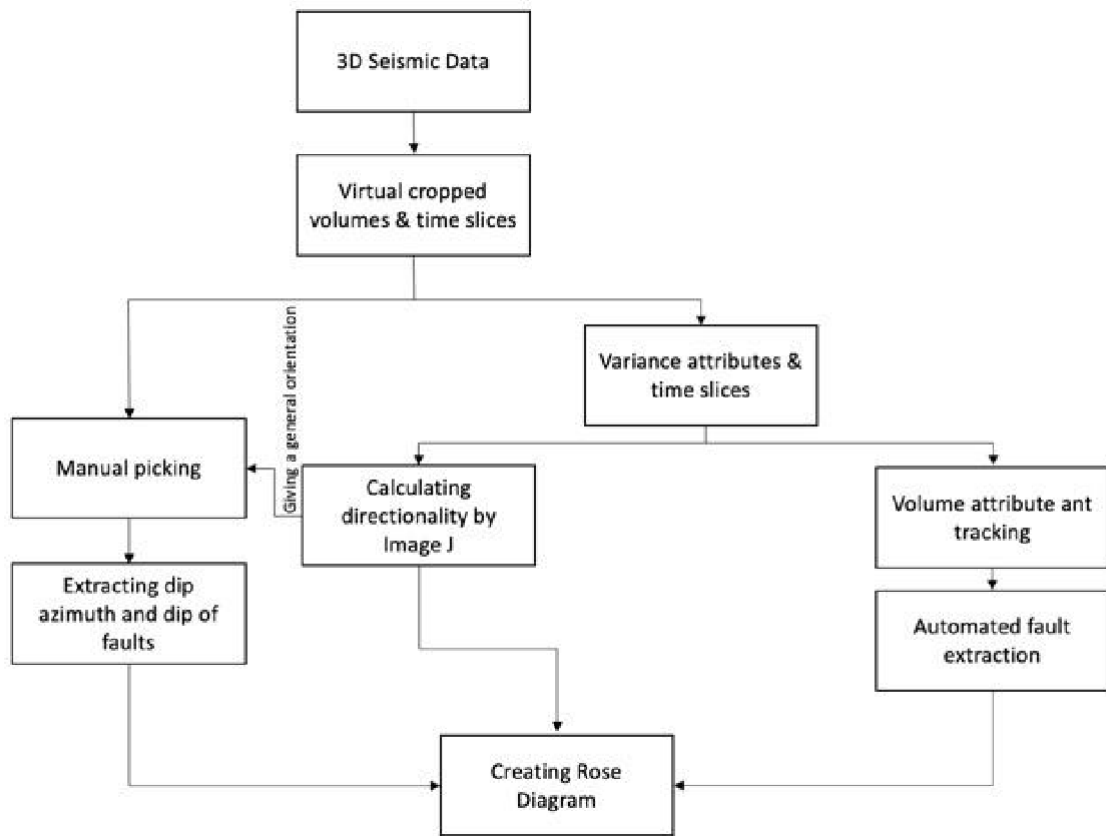
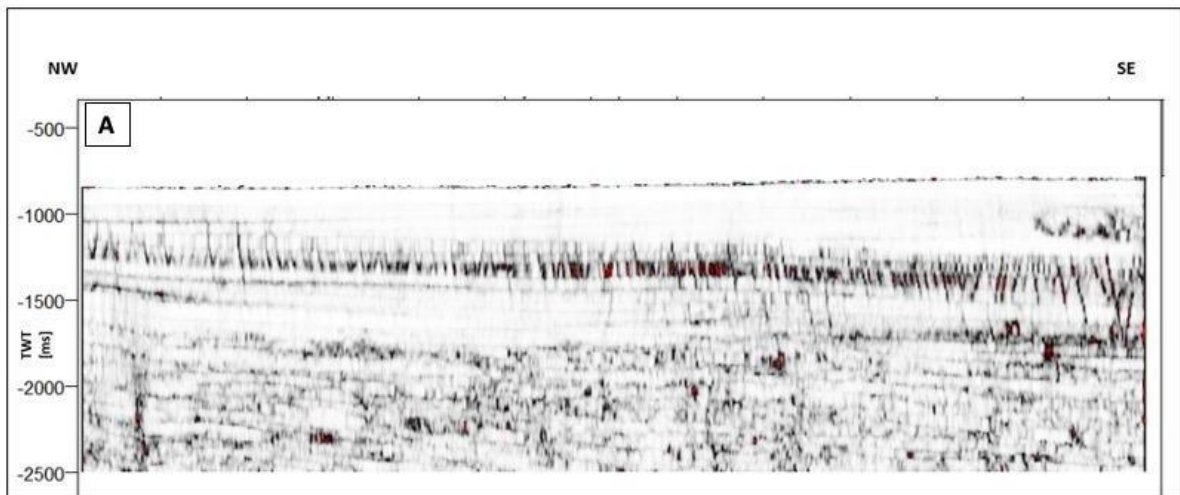
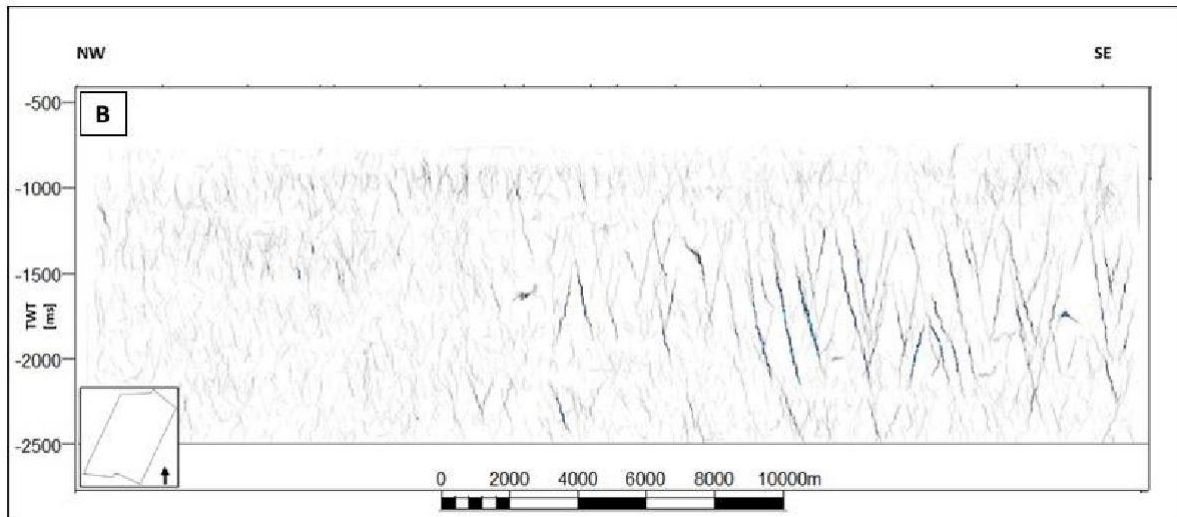


Fig. 4 Optimising 3D seismic-reflection analysis workflow.





**Fig.5** Vertical section of 3D seismic survey. (A) Seismic variance and (B) Ant tracking attribute.

### III. Result

#### Area 1

In area 1 (refer to figure 2 and figure 3a), the planform geometry varies through time. In the younger sediment (-1000ms TWT, Figure 6a), the planforms are linear / curve linear and the space between the faults is relatively big. In the older layers, the number of new faults is increasing and it formed in between the gaps of the earlier faults, resulting in increasing of the proportion of linkages which led to increasing the degree of maturity when the close-tips proportion more than the open-tips<sup>1</sup>. The morphology also changes from linear / curve linear to rectangle, radial and polygonal forms. Furthermore, the radial pattern appeared in the area where the pockmarks were concentrated (Figure 6b-c). In the older layers (-2300ms TWT in Figure 6d), the faults were re-oriented and formed hard-linked polygonal planform.

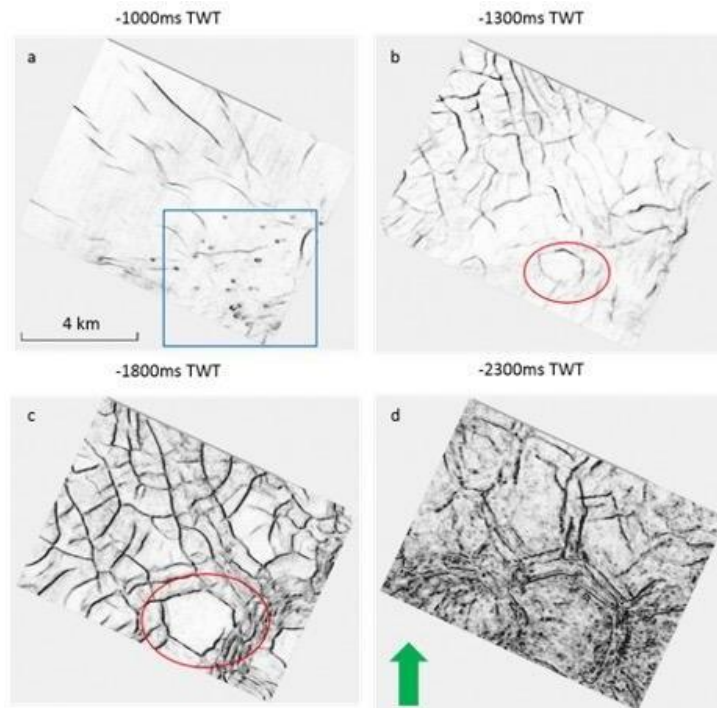


**Fig.6** Morphological development of area 1. The blue rectangle is the pockmarks area and the red circle is a radial pattern formed. These pockmarks are associated with the fault system indicating the fluid migration.

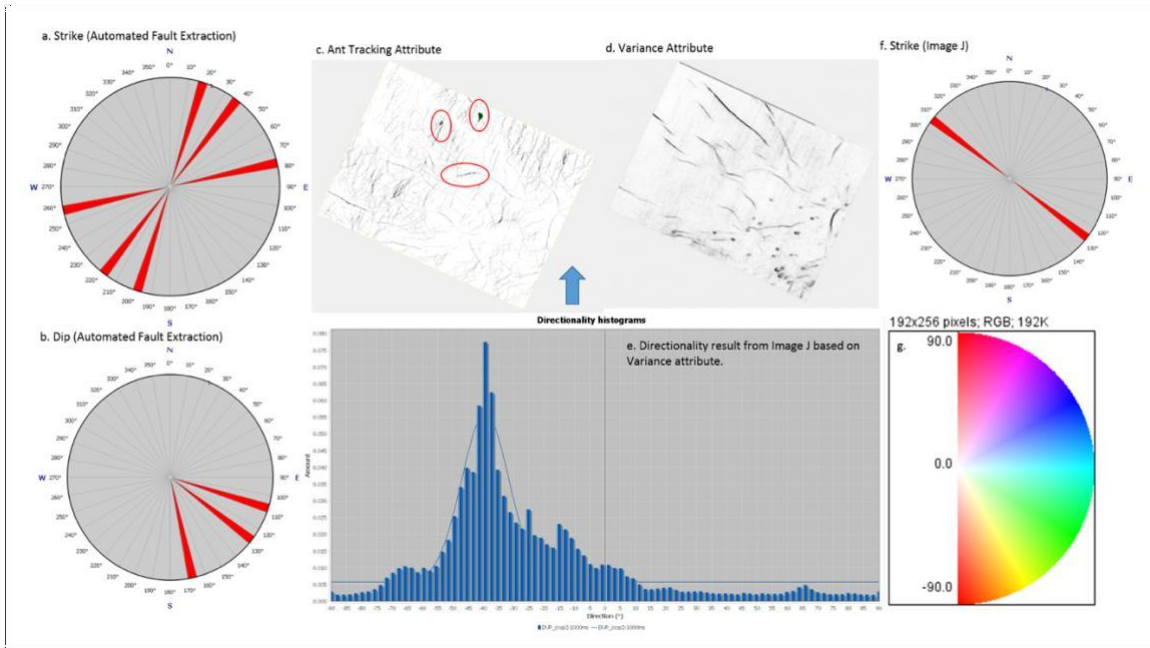


**Fig.7** The PFS directionality in younger sediment (-1000ms TWT). Figure a-b: strikes and dip direction obtained from automated fault extraction based on the ant tracking attribute (only shows 3 faults in this time slice on Figure c). Figure f: a strike of the preferred direction of Image J based on the variance attribute on figure d (the angle is adjusted towards north). Figure e: the directionality histogram produced by Image J with the peak  $-39.34^{\circ}$ . Figure g: the colour wheel of Image J. Rose diagrams created by using GeoRose software.

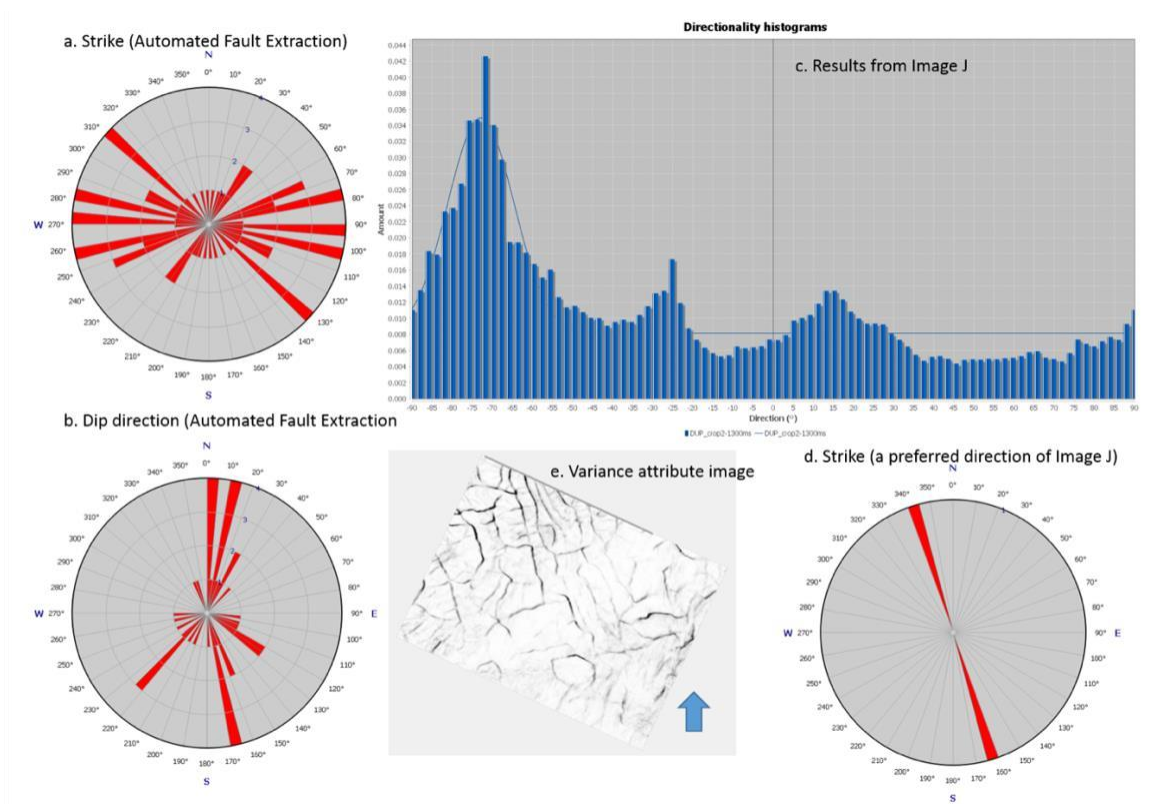


**Fig.8** Orientation of PFS at time interval of -1300ms TWT. (a-b) strikes and dip direction obtained from automated fault extraction which represent 41 faults at this time slice. (c) The directionality histogram produced by Image J with the peak of  $-72.85^{\circ}$  based on (e) the variance attribute image and d: a strike of the preferred direction of Image J (the angle is adjusted towards north).

The direction of polygonal faults varies within the stratigraphy. For instance, the PFS in the younger layer (-1000ms TWT) have preferred strikes of  $15^{\circ}$  to  $20^{\circ}$ ,  $35^{\circ}$  to  $40^{\circ}$  and  $75^{\circ}$  to  $80^{\circ}$  and dipping towards SE (Figure 7a- b). These values are generated by automated fault extraction of the ant tracking attribute, which cannot be observed in the variance attribute, whereas the result shown by Image J give a preferred direction of  $125^{\circ}$  to  $130^{\circ}$  based on the variance attribute. The histogram (Figure 7e) illustrates several orientations of the structures appeared on the image of variance attribute. The highest peak indicates the dominant direction of the structures. In this case, the peak point is  $-39.34^{\circ}$  which is referred to the colour wheel (Figure 7g). The  $0^{\circ}$  angle is represented by the east direction and the orientation is counter clockwise (for positive angles) and clockwise (for negative angles). Therefore, it requires an adjustment toward north direction to generate the strike of this angle.

In the deeper layers (Figure 8), the faults at -1300ms TWT have orientations with dominant strikes of  $75^{\circ}$  to  $80^{\circ}$ ,  $90^{\circ}$  to  $100^{\circ}$ ,  $130^{\circ}$  to  $135^{\circ}$  which were obtained from automated fault extraction and  $160^{\circ}$  to  $165^{\circ}$  dipping towards N-NE and SE processed by image J. Overall, the polygonal fault system in area 1 is dominantly dipping to NE and NW. The automated fault extraction recorded dominant strikes of  $60^{\circ}$  to  $65^{\circ}$  and  $150^{\circ}$  to  $175^{\circ}$  with orthogonal and random intersections (Figure 9a), whereas from the manual interpretation method, there are two preferred directions of approximately  $35^{\circ}$  to  $40^{\circ}$  and  $165^{\circ}$  to  $170^{\circ}$  (Figure 9b) and Image J recorded a preferred strike of about  $155^{\circ}$  to  $160^{\circ}$  (Figure 9c).

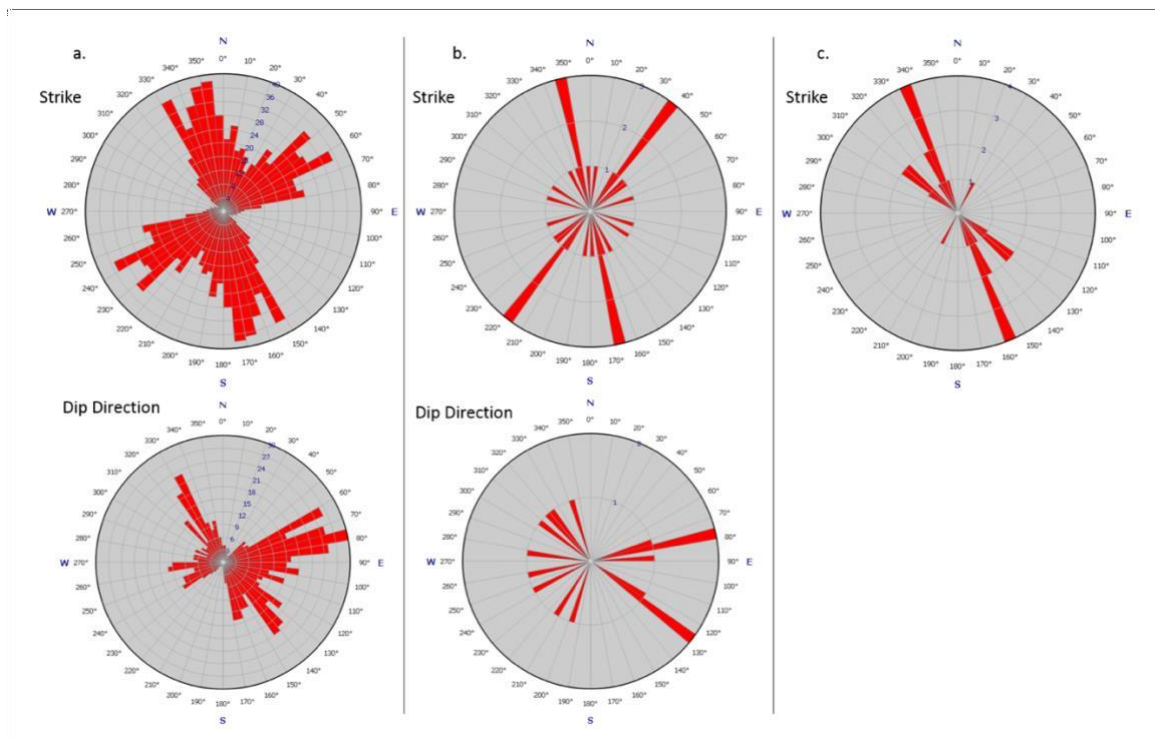


**Fig.9** Overall orientation of PFS in area 1. (a) Strike and dip direction obtained from automated fault extraction which represent 644 faults in all time slices (-1000ms TWT to -2300ms TWT). (b) Strike and dip direction obtained from manual interpretation which only contains 16 faults and (c): the preferred directions produced by the directionality histogram of Image J (from all 14 time slices, -1000ms to -2300ms TWT).

## Area 2

The planform geometry of the younger layer in area 2 (refer to figure 2 and figure 3b) is dominated by curve linear shapes. The radial to concentric patterns is clearly visible around the pockmarks area (Figure 10a). The presence of pockmarks in the younger layer indicates that there were many paths for fluids to migrate upwards and these also affect the directionality of polygonal faults. In addition, the maturity increases within the time as more faults were formed and joined orthogonally or randomly.

The polygonal faults in this area have various orientations due to the radial pattern. In the younger layers (-1000ms TWT), both manual interpretation and Image J show similar results with a preferred strikes of  $50^{\circ}$  to  $55^{\circ}$ , however more directions are illustrated in the manual interpretation (Figure 11). Towards the older layers, the data describe a wide range of strike directions as the faults are concentric-oriented. There are some different orientations between the manual interpretation, Image J and the automated fault extraction results particularly concentrated at the NW-SE strikes (Figure 12). However, the dominant trend is similar in

which most polygonalfaults have orientation of NNE-SSW and dipping towards ESE.

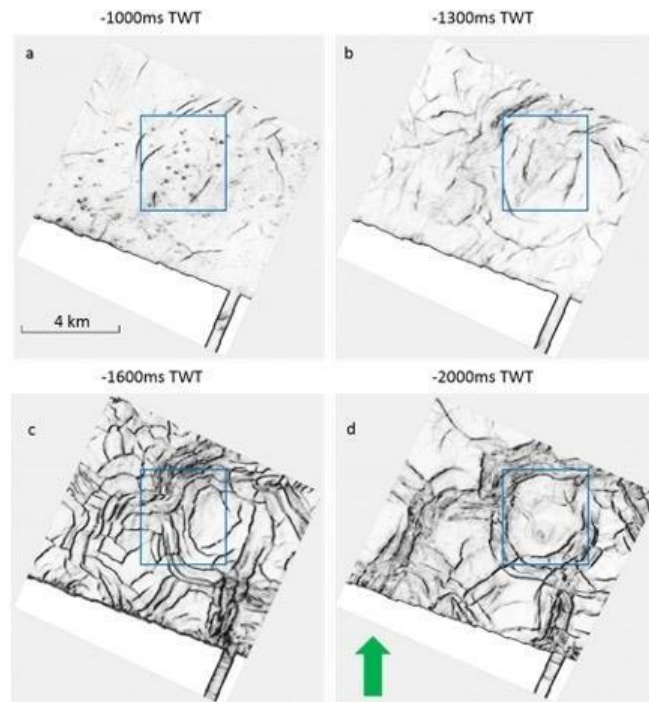


**Fig.10** Planform geometry changed from curve linear (a-b) to radial / concentric forms (c-d) in different time slices. Blue rectangles: the pockmarks cluster where the radial patterns formed. These radial patterns were growing and linked to each other.

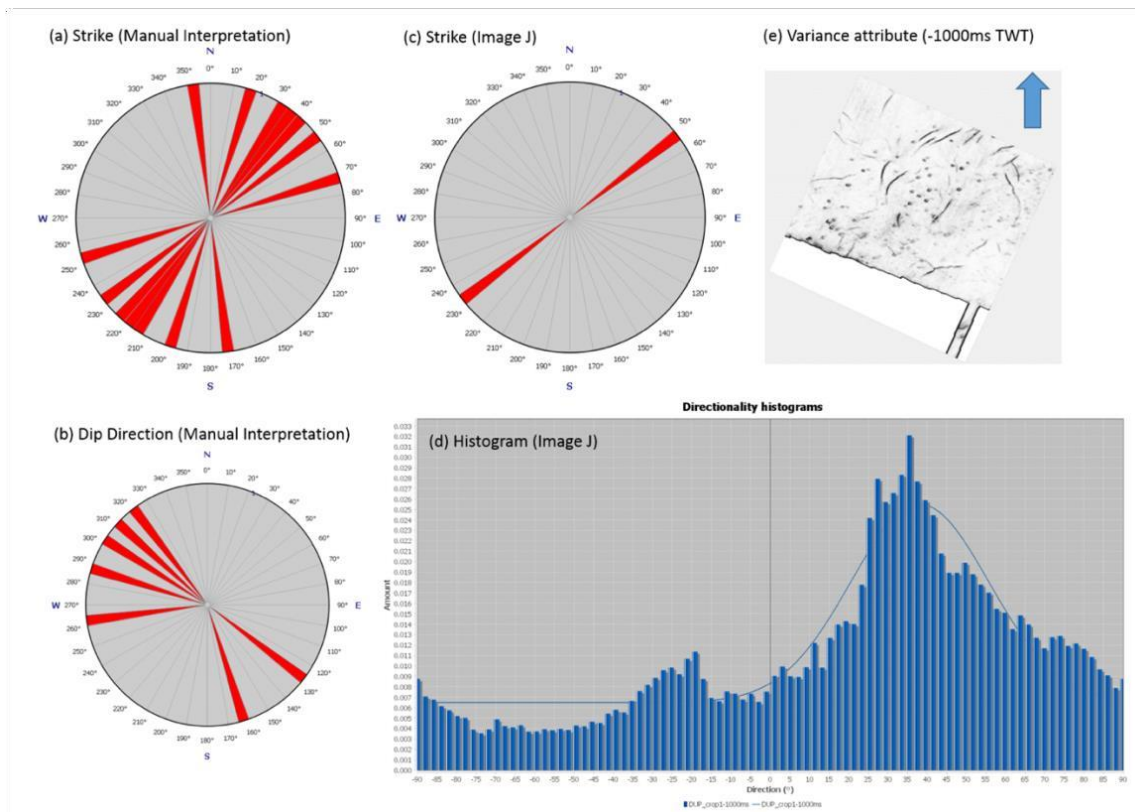


**Fig.11** PFS orientation at the younger sediments (-1000ms TWT). (a) and (b): strike-dip direction obtained from the manual interpretation which represent 7 faults. (c) and (d): strike and histogram obtained from Image J based on variance image (e). The highest peak of histogram shows the value of 38.14°.

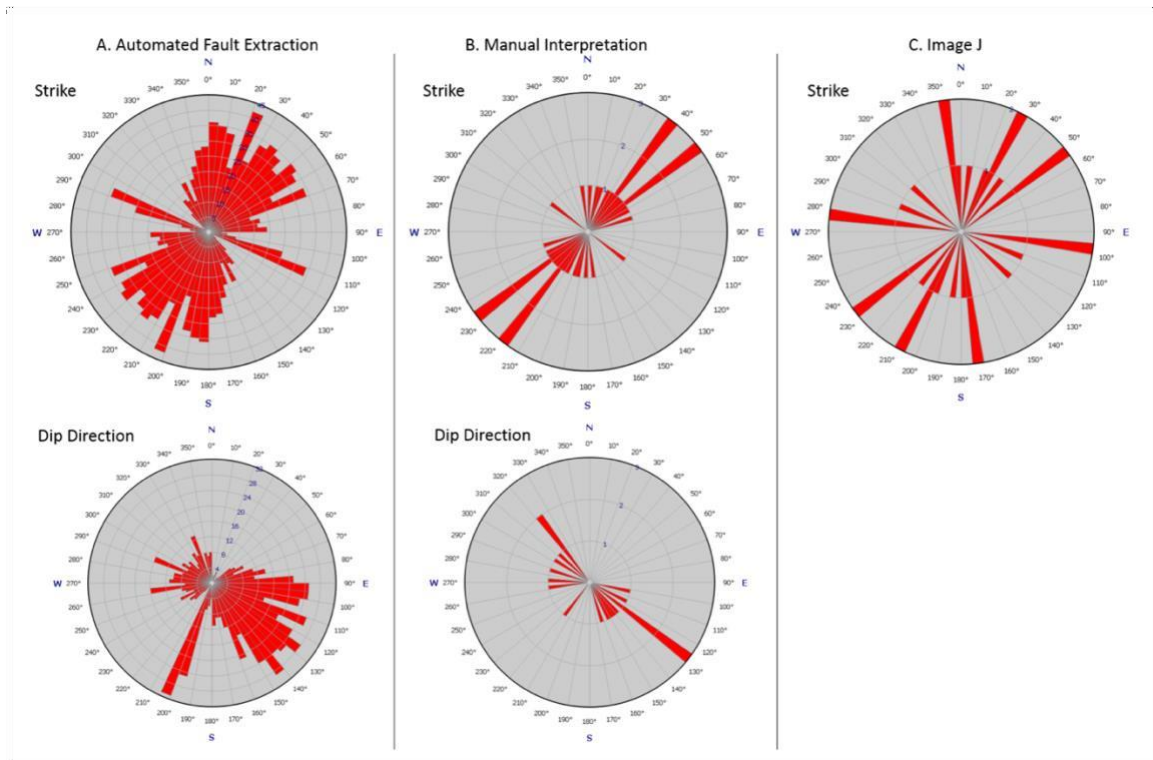


**Fig.12** Overall orientation of PFS in area 2. (A) The results from automated fault extraction represents 758 faults whereas (B) the manual interpretation only shows 18 faults and (C) Image J covers 14 time slices of variance attribute (from -1000ms to -2300ms TWT).

### Area 3

Area 3 is located in the eastern part (refer to figure 2 and figure 3c). The PFS are visible in the whole area within the interval of -1252ms to -2100ms TWT. The morphology of the faults is dominated with curve linear in the younger layer and likely to form a rectangular planform in the older layers (Figure 13). More linkages formed in the southern part of this area. Towards the deeper layers, the PFS in the northern part were begun to disappear at about -1800ms TWT. In addition, the maturity also increases within the time.

The orientations of faults in this area were dominated by two trends NE and SE with the preferred strikes of approximately  $60^{\circ}$  to  $75^{\circ}$  and  $165^{\circ}$  to  $170^{\circ}$ . However, Image J was not able to detect the major strike in the NW- SE direction. Most of the faults are dipping towards SE, some are dipping to NE and few others are dipping towards SW. Some of the orthogonal intersections can be found in this area (Figure 14).

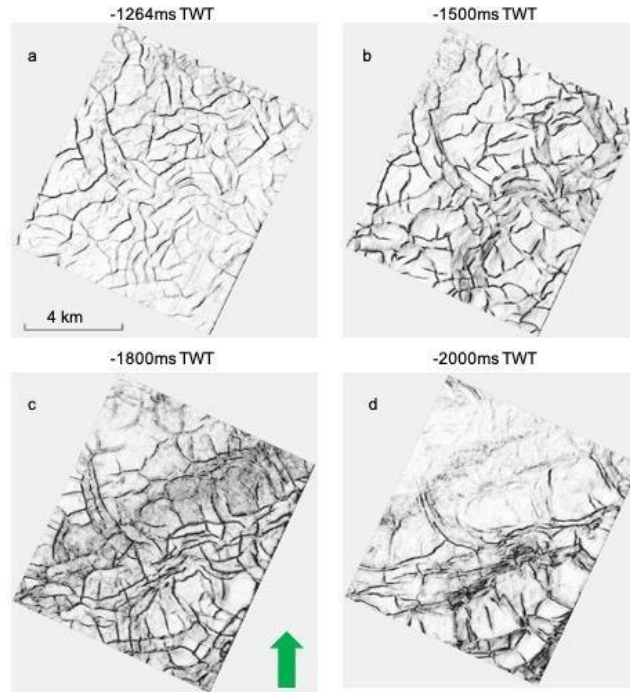


**Fig.13** Planform geometry changed from curve linear (a) to rectangle forms (b-d) in different time slices. In the older layers (c-d), the polygonal faults of the northern area were reducing whereas there are more close-tips found in the southern part.

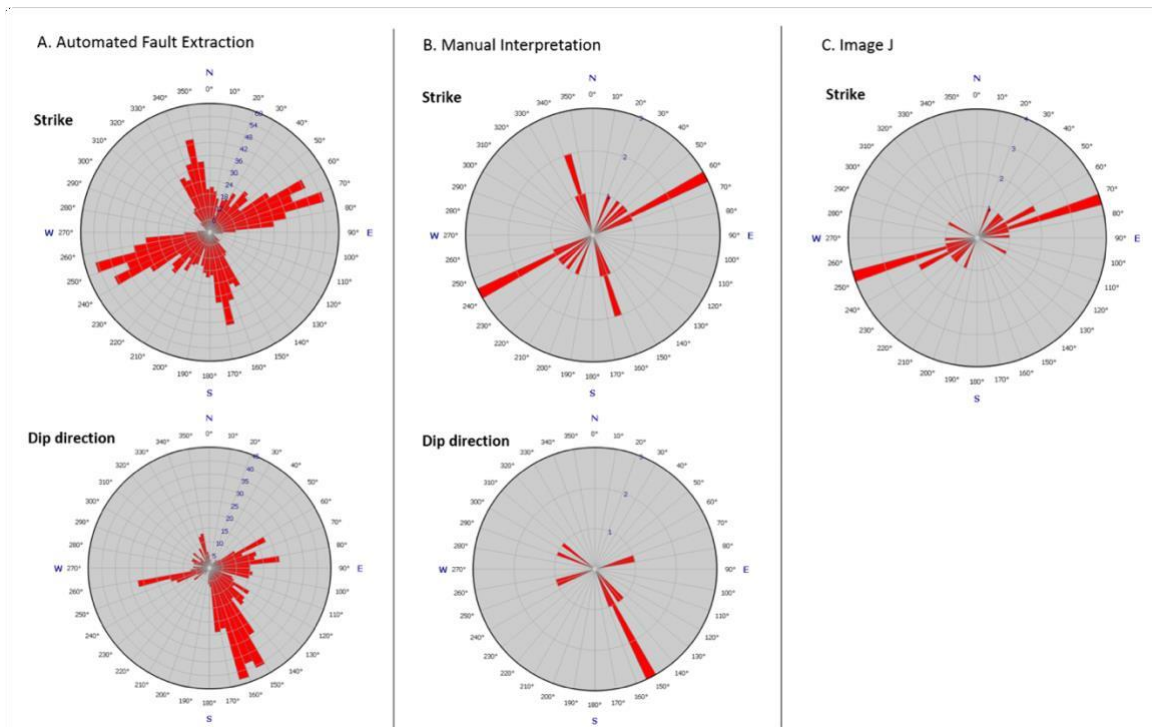


**Fig.14** Orientation of PFS in area 3. (A) The results from automated fault extraction represents 690 faults whereas (B) the manual interpretation only shows 12 faults and (C) Image J covers 14 time slices of variance attribute (from -1000ms to -2300ms TWT).

#### Area 4

Area 4.1 is located in the northern part of area 4 (refer to figure 3d). The PFS in this area has the thinnest interval among other areas and it lies in the shallower stratigraphic units. The polygonal faults can be observed

clearly in the entire area within the interval of -1152ms to -1300ms TWT. However, by using ant tracking, some faults are still detected in the very young sediments (Figure 15a). These faults show the same major trend of the underlying units. In general, the planform geometry in this area is more regularly organized than in the southern part (area 4.2). Most of the faults formed rectangular patterns (Figure 15c-d). The hard-linked between the faults were increasing during the time forming a mature system in this shallow tier yet then the PFS were begun to disappear at the interval of -1340ms TWT.

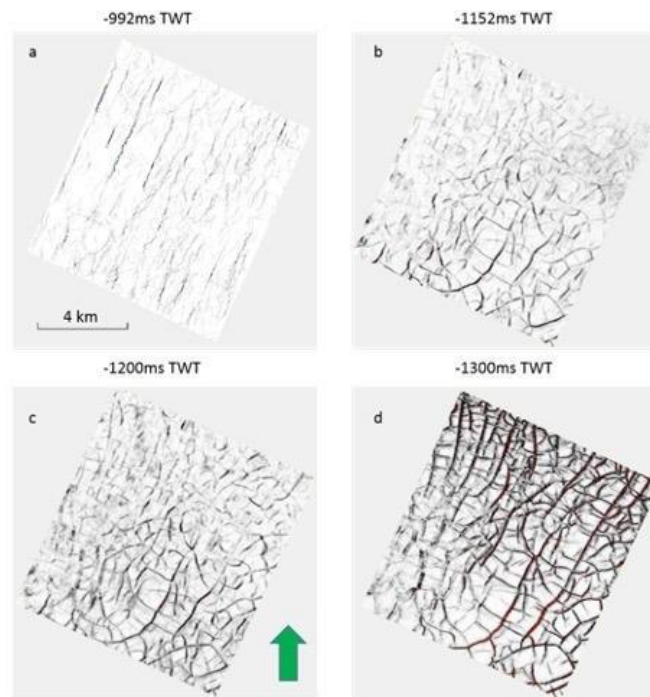


**Fig.15** (a) Ant tracking gives a better visualization of PFS in the younger sediments which cannot be observed in the variance attribute. (b-d) are the variance attributes. The PFS found were dominated by the rectangular patterns. The NE-SW is the major trend identified in the given intervals and some new trends were also present in the older sediments.

The orientation in the younger sediment (in the interval around -992msTWT) can be identified clearly through the ant tracking as it is shown in the figure 16e. Most of the faults show a dominant trend about NE-SW with the preferred direction of approximately  $20^{\circ}$  to  $30^{\circ}$ . This direction generated by both automated fault extraction which represents 17 faults in this layer (Figure 16a) and Image-J represents the direction in one time slice (Figure 16c). The overall orientations obtained from several time slices which are illustrated by three different methods are somewhat different. The results from automated fault extraction show that most of the faults are trending towards NE-SW with a preferred strike of about  $20^{\circ}$  to  $30^{\circ}$  and these results are based on 73 faults produced by the ant tracking (Figure 17A). Similarly, Image J also produced a preferred direction of approximately  $25^{\circ}$  to  $30^{\circ}$  based on six histograms from six different time slices (Figure 17C). In contrast, the manual interpretation depicted two dominant strikes of about  $35^{\circ}$  to  $40^{\circ}$  and  $120^{\circ}$  to  $125^{\circ}$  (Figure 17B). The results shown are based on 17 faults from the manual picking including the SE-NW direction which is not recorded in both the automated fault extraction and image J.

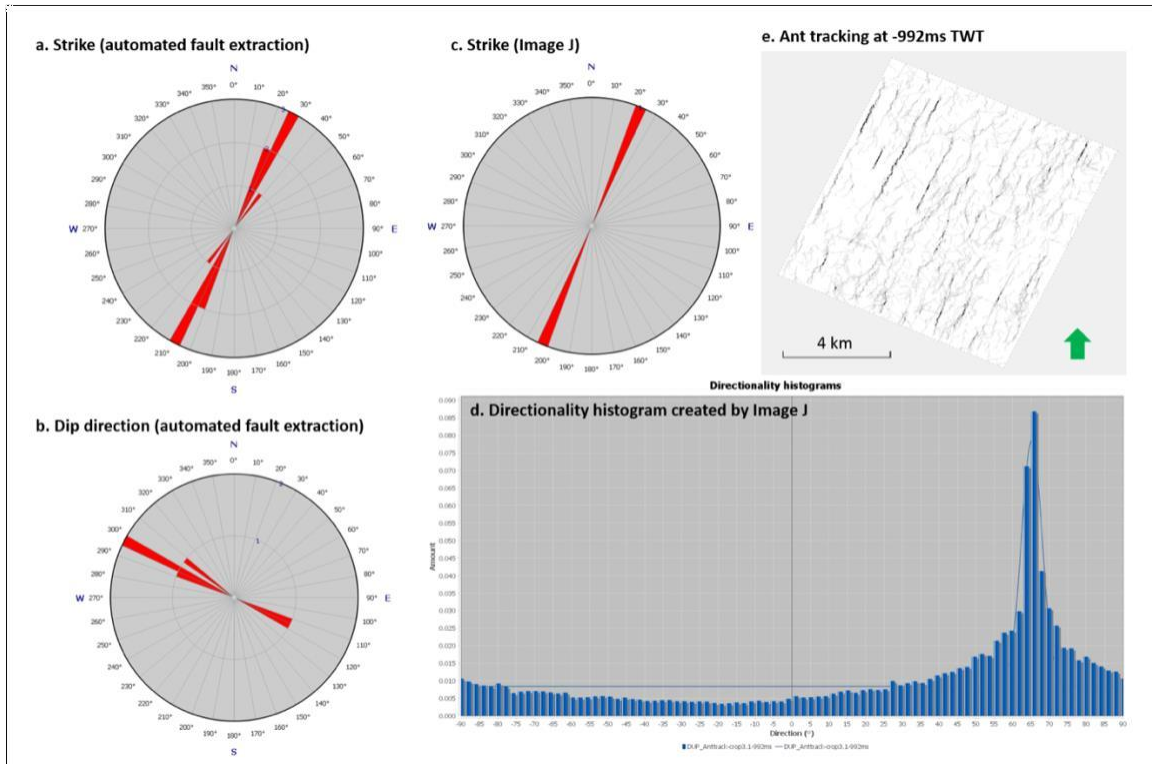


**Fig.16** Orientation of PFS in area 4.1 at interval of -992ms TWT. (a-b) Strike and dip direction obtained by automated fault extraction, (c) strike from Image J, and (d) the directionality histogram which represents the dominant direction of the structures appeared in the ant tracking at one time slice (e). The peak is  $65.2^{\circ}$  which is calculated from east (at  $0^{\circ}$  angle). The strike obtained by Image J has been adjusted from the histogram result.

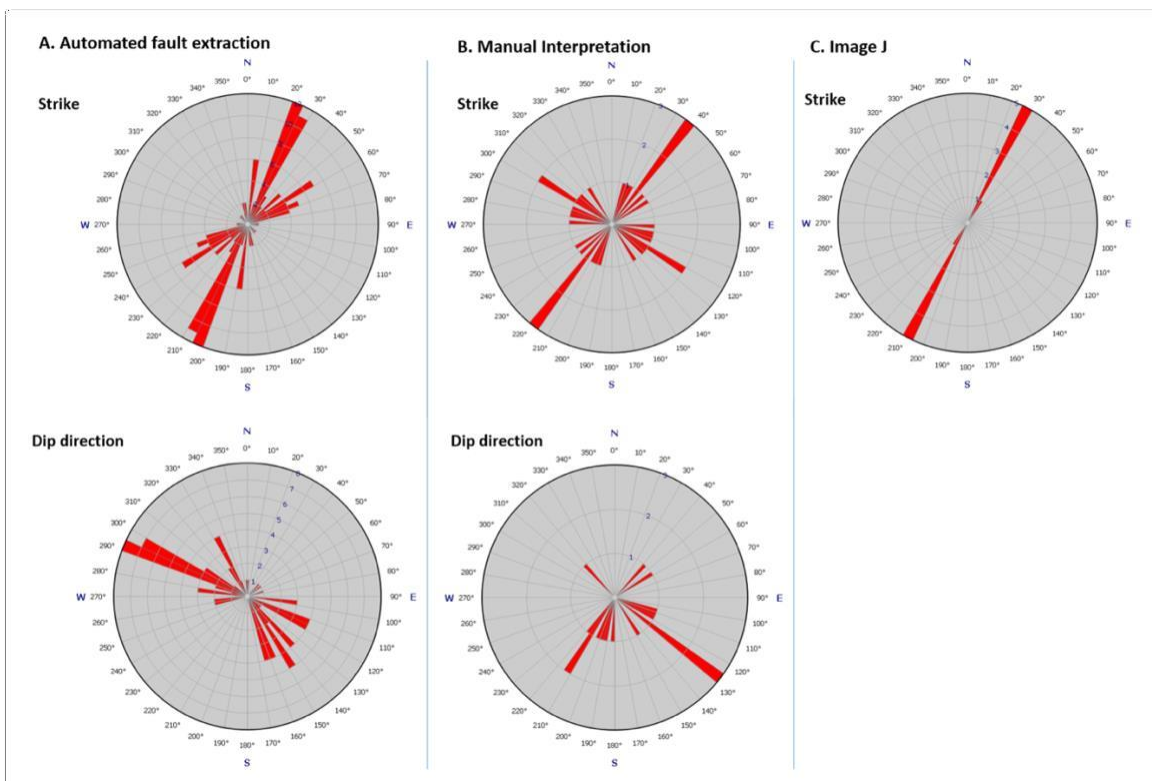


**Fig. 17** Overall orientation of PFS in area 4.1. (a) The results from automated fault extraction represents 73 faults whereas (b) the manual interpretation only shows 17 faults and (c) Image J covers 6 time slices of variance attribute (-1152ms to -1400ms TWT).

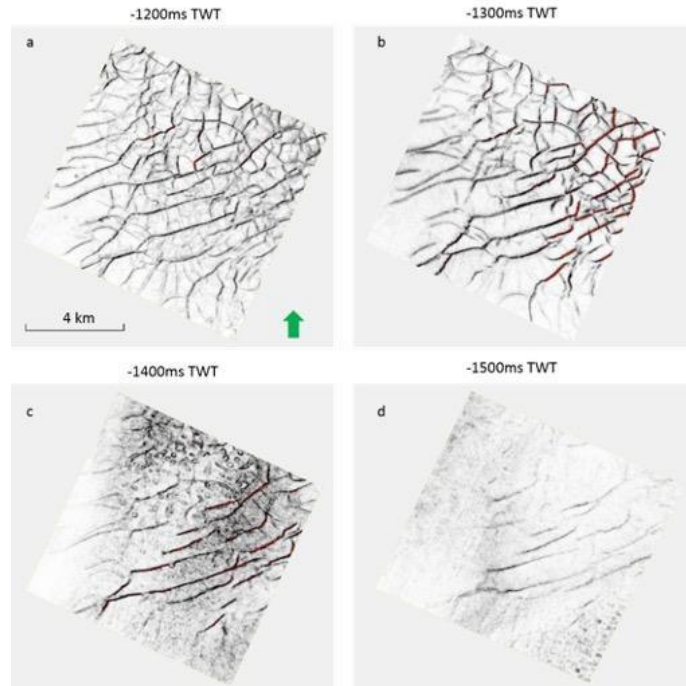


**Fig.18** Morphological development of PFS in area 4.2. More PFS are found in the younger sediments and decreasing towards the older sediments (a-d). Rectangular shapes are dominantly occurred in the shallow tier (a).

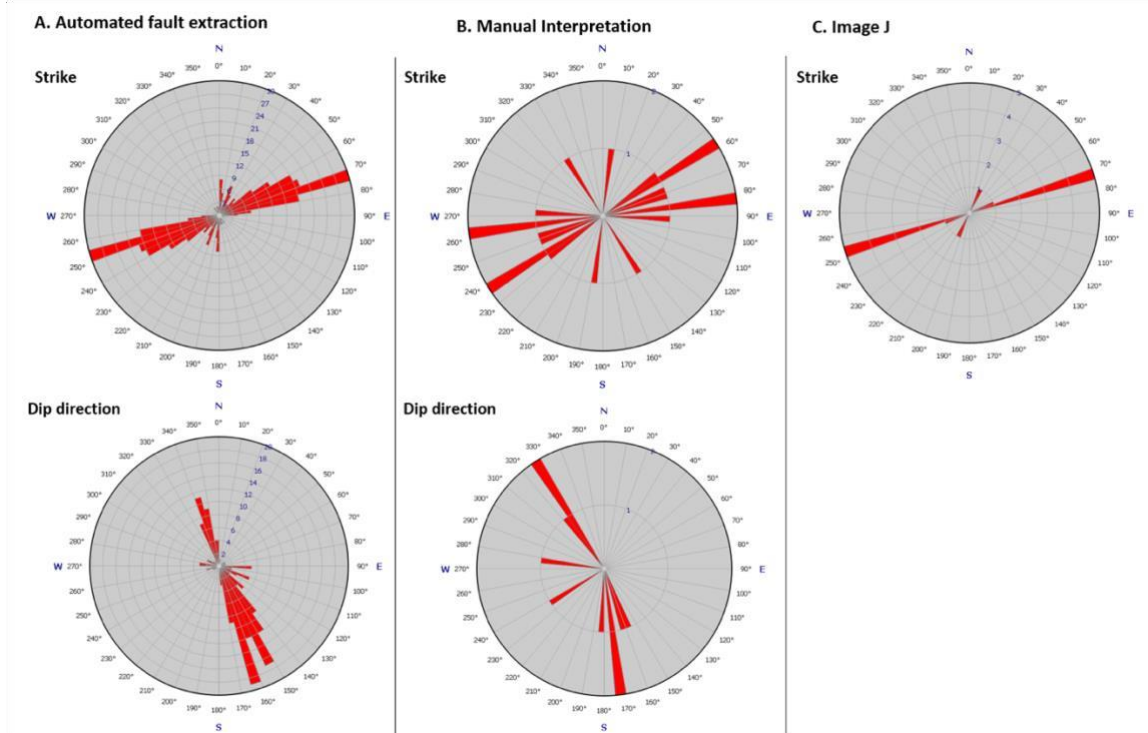


**Fig. 19** Orientation of PFS in area 4.2. (A) The results from automated fault extraction containing 170 faults. (B) Manual interpretation results represent 10 faults. (C) The result obtained by Image-J representing the preferred directions of 14 time slices (from -1100ms to -1600ms TWT).

The PFS are visible in the entire area 4.2 within the interval of -1120ms and started to decrease in the interval of -1400ms TWT. These PFS cover about 300ms TWT intervals. The planform geometry changed from rectangular and / or random forms to linear patterns from the younger to older stratigraphy units (Figure 18). The hard-linked of PFS are decreasing through time. The more mature system occurred within the interval of -1200ms to -1300ms TWT than in the older layers. The polygonal faults show a dominant direction

around  $70^{\circ}$  and are generally dipping towards SE (Figure 19). The automated fault extraction obtained a similar result with Image J, whereas the manual interpretation resulted two preferred strikes about  $55^{\circ}$  and  $80^{\circ}$ .

According to the observation, most of the study areas show the same PFS trend where the PFS are likely to have a preferred direction towards NE-SW and dipping to SE. However, some PFS in area 1 and 2 in particular also have NW trend.

#### IV. Discussion

The similarity and/or the variation in directionality from three methods provide an extensive interpretation of PFS orientation. Image J software provides a preferred direction of the structures of the image obtained from variance or ant tracking attribute which can help to decide which faults to pick for manual picking. Nevertheless, the directionality depends on the resolution of the image. For low quality resolution, Image J is not able to capture all structures in the image. Another problem of Image J is that it cannot distinguish between fault and seismic artifacts (Figure 20).

In contrast, the manual interpretation method allows us to choose faults that are visible in the seismic section, analyse the fault's structure and construct the fault's plane. However, the orientation obtained from manual interpretation in this case is likely to depend on the number of faults that are visible on the variance attribute. For a large data containing numerous of faults and forming polygonal platform, manual picking is a very complex and monotonous method.

The third method is automated fault extraction which extracts the faults from the ant tracking attribute. To apply this method, it requires a sensitive attribute such as variance attribute before applying the ant tracker in order to have an optimal result. The ant tracking attribute provides more fault data (not only major faults as it is shown in the variance attribute).

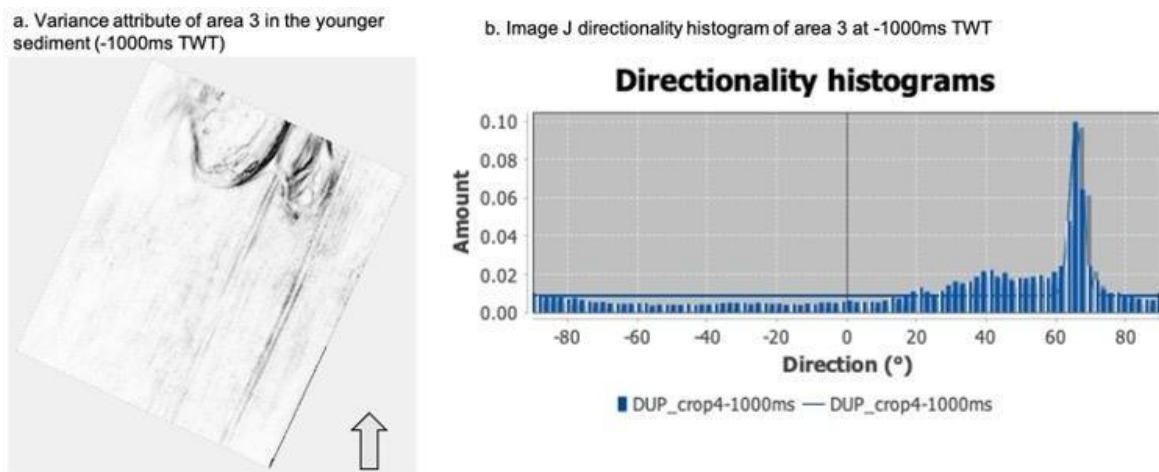


**Fig.20** (a) indicating seismic artifacts in area 3, (b) the directionality produced by Image J of the structures on that time slice image indicating a preferred direction of  $65.99^{\circ}$  from east direction.

There are some interesting findings in this study. For instance, the result shown in figure 17 (area 4). More SE-NW fault orientations are visible in the manual interpretation than in image J or automated fault extraction. The variance attributes in figure 15 c and d describe the NE-SW major faults intersecting with several SE-NW minor faults forming a rectangular pattern, further support this result. Another example, Image J recorded the trend of the major structures with strikes of about  $125^{\circ}$  to  $130^{\circ}$  in area 1 at the interval of -1000ms TWT, whereas automated fault extraction recorded different preferential orientations of  $15^{\circ}$  to  $20^{\circ}$ ,  $35^{\circ}$  to  $45^{\circ}$  and  $75^{\circ}$  to  $80^{\circ}$  (Figure 7). Despite the fact that both the ant tracker and variance attributes show NE-SW and SE-NW orientations, the image J is unable to perform the orientation of NE-SW faults as shown on the automated fault extraction result, while the automated fault extraction is unable to record SE-NW orientation. Moreover, manual picking on the seismic 3D data in this younger layer cannot be done due to the difficulty to track the fault's path. In area 3 (Figure 14), More faults recorded by automated fault extraction with the orientations of NE-SW and SE-NW. Image J and manual interpretation were unable to perform the SE-NW fault orientation as many as automated fault extraction. This might be due to the declining of the polygonal faults in the northern part of the study area which mostly have NW trends, hence the faults do not appear clearly in the variance attribute image (Figure 13c-d).

In addition, the changes in morphology of polygonal faults are affected by the presence of pockmarks and the effect of stress anisotropy perturbing fault planform due to local changes in slope<sup>1</sup>. From the younger

layer to the older layer, the planforms change from linear/curve linear to rectangle and polygonal forms especially in area 1, 2 and 3. For instance, in the older layer of area 1 (Figure 6d), the faults tend to be reoriented and formed hard-linked intersections. This is perhaps due to the earlier growth of new faults which filled the gaps forming morerestricted tips and reduced the fault's displacement.

## V. Conclusion

Image J directionality is a useful tool to obtain a preferential orientation of polygonal faults and it is less time- consuming method. However, the result is highly depending on the clarity and resolution of the image used. Similarly, manual interpretation technique for polygonal faults allows us to illustrate and analyse the major fault's structure but it is a cumbersome activity especially with the hard-links formed along the faults. The automated fault extraction with ant tracking attribute is a remarkably effective method for the polygonal faults mapping. Ant tracker is able to enhance faults interpretation in the 3D seismic data and fault geometry (dip, dip azimuth) can be easily extracted. However, before using the ant tracker, it is necessary to decrease the residue noise with a sensitive attribute, such as the variance attribute. The overall outcome shows some differences and similarity in directionality of PFS indicating the limitation of each method.

## References

- [1]. Cartwright, J., 2011. Diagenetically induced shear failure of fine-grained sediments and the development of polygonal fault systems. *Marine and Petroleum Geology - MAR PETROL GEOL*, 28, p.1593-1610. DOI: 10.1016/j.marpetgeo.2011.06.004.
- [2]. Cartwright, J., Dewhurst, D., 1998. Layer-Bound compaction faults in fine-grained sediments. *Bulletin of the Geological Society of America*, 110(10), p.1242 - 1257. DOI: 10.1130/0016-7606(1998)110<1242:LBCFIF>2.3.CO;2.
- [3]. Buckley, D.E, Grant, A.C., 1985. Faultlike features in abyssal plain sediments:possible dewatering structures. *Journal of Geophysical Research*, 90, p.9173 - 9180. DOI: 10.1029/JC090iC05p01973.
- [4]. Williams, S.R.J., 1987. Faulting in abyssal-plain sediments, Great Meteor East, Madeira Abyssal Plain. In: Weaver, P.P.E., Thomson, J. (Eds.), *Geology and Geochemistry of Abyssal Plains. Geological Society, London, Special Publications*, 31, p.87 - 104. DOI: 10.1144/GSL.SP.1987.031.01.08.
- [5]. Henriot, J., De Batist, M., Van Vaerenburgh, W., Verschuren, M., 1989. Seismic facies and clay tectonic features of the Ypresian clay in the southern North Sea. *Bulletin of the Belgian Geological Society*, 91, p.457 - 472.
- [6]. Cartwright, J., 1994a. Episodic basin-wide hydrofracturing of overpressured early Cenozoic mudrock sequences in the North Sea Basin. *Marine and Petroleum Geology*, 11(5), p.587 - 607. DOI: 10.1016/0264-8172(94)90070-1.
- [7]. Cartwright, J., 1994b. Episodic basin-wide fluid expulsion from geopressed shale sequences in the North Sea Basin. *Geology*, 22(5), p.447 - 450. DOI: 10.1130/0091-7613(1994)022<0447:EBWFEF>2.3.CO;2.
- [8]. Ghisetti, F., 2010. Seismic Interpretation, Prospects and Structural Analysis, Great South Basin. *Ministry of Economic Development New Zealand*, Unpublished Petroleum Report PR4173.
- [9]. Morley, C.K., Maczak, A., Rungprom, T., Ghosh, J., Cartwright, J.A., Bertoni, C., Panpichityota, N., 2017. New style of honeycomb structures revealed on 3D seismic data indicate widespread diagenesis offshore Great South Basin, New Zealand. *Marine and Petroleum Geology*, 86, p.140-154. DOI: 10.1016/j.marpetgeo.2017.05.035.
- [10]. Berndt, Christian, 2006. Focused fluid flow on continental margins. *Philosophical transactions. Series A, Mathematical, physical, and engineering sciences*, 363, p.2855-71. DOI: 10.1098/rsta.2005.1666.
- [11]. Higgs, W., McClay, K., 1993. Analogue sandbox modelling of Miocene extensional faulting in the Outer Moray Firth. *Tectonics and Sequence Stratigraphy, Geological Society, London, Special Publications*, 71(1), p.141-162. DOI: 10.1144/GSL.SP.1993.071.01.07.
- [12]. Henriot, J.-P., De Batist, M., Verschuren, M., 1991. Early fracturing of Paleogene clays, southernmost North Sea: relevance to mechanisms of primary hydrocarbon migration. In: Spencer, A.M. (Eds). *Generation, Accumulation and Production of Europe's Hydrocarbon, EAPG Special Publication No 1, Oxford University Press*, p.217-227.
- [13]. Watterson, J., Walsh, J., Nicol, A., Nell, P.A.R., Bretan, P.G., 2000. Geometry and origin of a polygonal fault system. *Journal of Geological Society*, 157(1), p.151-162. DOI: 10.1144/jgs.157.1.151.
- [14]. Gouly, N., 2001. Polygonal fault networks in fine-grained sediments - An alternative to the syneresis mechanism. *First Break*, 19, p.69-73. DOI: 10.1046/j.1365-2397.2001.00137.x.
- [15]. Kessler, M., Werner, B., 2003. Self-organization of storted patterned ground. *Science*, 299, p.380-383. DOI: 10.1126/science.1077309.
- [16]. Faugeres, J.-C., Stow, D., Imbert, P., Viana, A., 1999. Seismic features diagnostic of contourite drifts. *Marine Geology*, 162, p.1-38. DOI: 10.1016/S0025-3227(99)00068-7.
- [17]. Stuevold, L., Faereth, R., Arnsen, L., Cartwright, J.A., Moller, N., 2003. Polygonal faults in the Ormen Lange field. In: Van Rensibergen, P., Hillis, R.R., Morley, C.K.(Eds.), *Subsurface Sediment Mobilization. Geological Society, London, Special Publications*, 216, p.263-281.
- [18]. Tinevez, J.-Y., 2020. *ImageJ*. [Online]. Available at: <https://imagej.net/Directionality>. [Accessed 6 August 2020].
- [19]. Chopra, S., Marfurt, K.J., 2007a. Volumetric curvature attributes add value to 3D seismic data interpretation. *The Leading Edge*, 26(7), p.856-867. DOI: 10.1190/1.2756864.